THE JOURNAL OF PHYSICAL CHEMISTRY C

pubs.acs.org/JPCC Article

Gas Evolution in Li-Ion Batteries: Modeling Ethylene Carbonate Decomposition on $LiCoO_2$ in the Presence of Surface Magnetism

Mallory R. Fuhst and Donald J. Siegel*

Cite This: *J. Phys. Chem. C* 2020, 124, 24097−24104 Read Online

ACCESS | Metrics & More | Article Recommendations | Supporting Information

ABSTRACT: Decomposition of liquid electrolytes used in Li-ion batteries can result in the formation of gaseous species and the release of flammable solvent vapor. These undesirable "gassing" reactions can be mediated by interactions between the electrode surfaces and the electrolyte. At present, the detailed mechanisms responsible for electrolyte gassing are not well understood. Here, first-principles calculations are used to characterize the thermodynamics and kinetics of potential gas-forming reactions that involve surface-mediated decomposition of ethylene carbonate (EC)—a commonly used electrolyte solvent—at the $(10\bar{1}4)$ surface of a $LiCoO_2$ (LCO) cathode. The magnetic ordering of the $(10\bar{1}4)$ surface was explicitly taken into account. Comparisons of EC adsorption on nonmagnetic, ferromagnetic, and antiferromagnetic surface orderings reveal differences in the adsorption geometry and reaction energetics. The antiferromagnetic surface exhibited the lowest surface energy overall; EC adsorption on this surface preferentially occurs on Li sites. In contrast, the nonmagnetic surface exhibits a stronger attraction for EC—adsorption is 0.5 eV more exothermic per molecule than for the antiferromagnetic surface—and adsorption occurs on Co sites. The thermodynamic driving force for EC decomposition on the antiferromagnetic surface was predicted for several potential reaction products resulting from more than 30 bond-breaking scenarios. The most exothermic of these reactions results in the formation of CO_2 and acetaldehyde (C_2H_4O), gaseous products that have been observed in prior experiments. Nevertheless, an evaluation of the minimum energy path for CO_2/C_2H_4O formation on fully lithiated LCO reveals a large reaction barrier for this process, implying a kinetically limited reaction. These data suggest that the rate of solvent decomposition at the cathode may be maximized in the charged state, where LCO is partially delithiated.

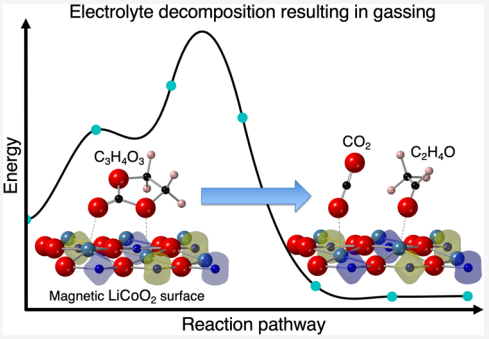

INTRODUCTION

Li-ion batteries represent the state of the art in energy storage for portable electronics. No other battery chemistry has been demonstrated to surpass its favorable combination of energy density and cycle life.[1−3]

Nevertheless, improving the safety of Li-ion batteries remains an important goal.[1,4] For example, the formation of gaseous species resulting from decomposition of the liquid electrolyte can result in the release (*i.e.*, venting) of flammable solvent vapor.[5−9] Previous studies have suggested that gas evolution is impacted by the chemistry of the lithium metal oxide cathode.[4,6−11] Interactions between the cathode surface and species in the electrolyte could mediate the decomposition of the electrolyte, resulting in gas formation. However, the exact reaction mechanisms responsible for electrolyte decomposition at the cathode surface are not well understood.

The present study investigates how the surface of a $LiCoO_2$ (LCO) cathode could mediate electrolyte decomposition. LCO is an intercalation cathode consisting of alternating layers of CoO_2 and Li ions; Figure 1 shows the crystal structure of the hexagonal unit cell. Due to its high energy density, LCO is a common cathode material in commercial batteries, particularly portable electronics.[2] However, in comparing six cathode materials during thermal abuse studies, Roth found that LCO had higher reaction rates, higher enthalpies of reaction, and the lowest onset temperature for gassing reactions.[4] Also, the addition of electrolyte additives yielded the smallest improvements in gassing behavior in cells based on LCO. Consequently, the propensity for LCO to facilitate electrolyte gassing has limited its use in some battery applications.

It has been reported that the surfaces of electrodes can promote electrolyte decomposition.[6−9,11,12] The most prevalent surfaces of LCO crystallites are the (0001), $(10\bar{1}4)$, and $(01\bar{1}2)$ surfaces.[13−15] Of these, the polar (0001) surface terminating in an oxygen layer has been reported to comprise the largest area fraction. This surface does not participate in Li intercalation.[13] Since Li shuttling during charge/discharge is

Received: August 18, 2020
Revised: October 12, 2020
Published: October 27, 2020

https://dx.doi.org/10.1021/acs.jpcc.0c07550
J. Phys. Chem. C 2020, 124, 24097−24104

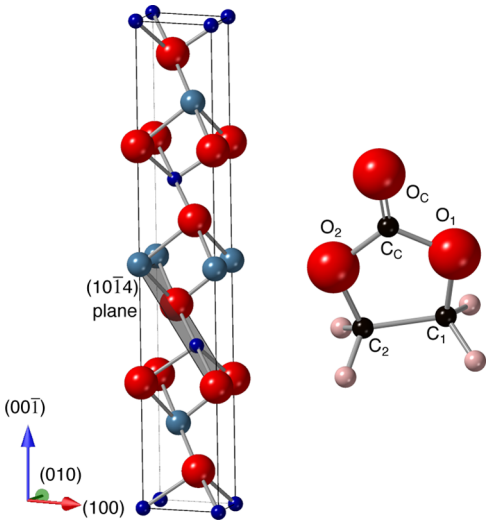

Figure 1. Structure of hexagonal LCO (left) and EC (right). The (10$\bar{1}$4) plane of LCO is shown within the unit cell. Li, Co, C, H, and O are shown in teal, blue, black, pink, and red, respectively.

believed to contribute to electrolyte decomposition, this suggests that electrolyte interactions involving the (0001) surface may not contribute to gassing. Hence, the present study focuses on the (10$\bar{1}$4) surface; this surface is the second lowest in energy, is nonpolar, and is expected to contribute to lithium insertion/extraction from the cathode.[14,15] The (10$\bar{1}$4) plane is illustrated within the LCO hexagonal cell in Figure 1.

Recent studies have shown that some LCO surfaces exhibit unpaired spins on surface Co due to the disruption of the structure (*i.e.*, broken bonds) of the oxygen octahedron that would otherwise coordinate Co in bulk LCO.[14,15] In the bulk system, fully coordinated Co^{3+} adopt a low spin (nonmagnetic) state, but Co^{3+} ions at the surface may adopt intermediate or high spin states as a result of broken bonds. In particular, exposed Co^{3+} on the (10$\bar{1}$4) surface exhibit an intermediate spin state with magnetic moments of $\pm 2\ \mu_B$.[14−16] Allowing for unpaired spins on surface Co can lower the surface energy and may contribute to the reactivity of LCO toward electrolytes.

Li-ion batteries use liquid electrolytes consisting of a Li salt, an organic carbonate solvent, and various additives to improve performance. Ethylene carbonate (EC), a commonly used electrolyte solvent, is known to decompose at the anode; these decomposition products are a component in the solid electrolyte interphase.[11,17] The molecular structure of EC is illustrated in Figure 1. Oxidized carbonate species have been found on the cathode surface of LCO-based systems,[2,11,18] which presumably result from decomposition reactions occurring at the electrolyte/electrode interface.

The mechanisms that underlie electrolyte decomposition on LCO surfaces have been investigated in a few previous studies.[18−21] Tebbe *et al.* conducted a density functional theory (DFT) study on the decomposition of EC on the (10$\bar{1}$4) LCO surface, with and without the addition of other electrolyte molecules. Their study suggested that a high energy barrier to surface-mediated decomposition exists in the absence of a strong Lewis acid, such as PF_5.[19] However, this study did not account for unpaired spins on the electrode surface; furthermore, EC adsorption was limited to surface Co^{3+} ions. Later, Giordano *et al.* also conducted DFT studies to model EC reactivity with (10$\bar{1}$4) LCO and other common lithium metal oxide cathodes. Their study examined four potential reaction pathways and assumed a ferromagnetic ordering of surface Co^{3+}. They found that EC adsorption and dissociation through deprotonation was exothermic on LCO.[20] They also found that the driving force for EC dissociation at the surface increased as Li was removed from the electrode. Finally, Tamura *et al.* used first-principles molecular dynamics to study EC on the (11$\bar{2}$0) surface of LCO, observing EC adsorption on surface Co^{3+} ions and EC dissociation through ring opening at the surface.[21]

The present study builds on these earlier reports by using classical and first-principles techniques to characterize potential gassing reactions in Li-ion batteries. Specifically, the thermodynamics and kinetics of surface-mediated EC decomposition are probed on the (10$\bar{1}$4) surface of LCO. Following the methodology of Kumar *et al.* for solvent adsorption and decomposition, classical Monte Carlo (MC) calculations were used to screen hundreds of potential absorption geometries.[22,23] These results, supplemented with geometries from the literature and chemical intuition, were used to down-select more than 30 geometries that were subsequently refined with DFT calculations. The magnetic state of the LCO surface was explicitly taken into account by comparing the adsorption behavior of EC among three different magnetic orderings—nonmagnetic, ferromagnetic, and antiferromagnetic—with the antiferromagnetic ordering being the lowest in energy. Surface magnetism was found to have a large impact on the adsorption geometry and the reaction energetics. EC prefers to adsorb at surface Co sites on the nonmagnetic surface (the highest energy surface) but prefers Li sites in both ferromagnetic and antiferromagnetic states. In all cases, little charge transfer is observed, suggesting that van der Waals and electrostatic interactions dominate.

The thermodynamic driving force for EC decomposition was predicted for eight potential reaction products derived from over 30 different bond breaking scenarios. The most exothermic reaction investigated results in the formation of CO_2 and acetaldehyde (C_2H_4O) with an exothermic driving force of 0.85 eV/molecule. The observation of gaseous CO_2 as a reaction product is consistent with prior experiments.[5,18,24,25] In addition, Gauthier *et al.* have detected acetal groups at the LCO surface after cycling in an EC-based electrolyte.[18] Nudged elastic band (NEB) calculations were used to map out the minimum energy pathway for this decomposition reaction. A relatively large barrier was found, suggesting that this reaction will be kinetically limited. As previous studies have reported more rapid solvent decomposition kinetics upon delithiation of LCO and similar lithium metal oxides, it can be hypothesized that a smaller barrier—and faster decomposition rate—may exist in the (partially) delithiated state.[20,22,26]

METHODS

DFT calculations were performed using the Vienna *ab initio* Simulation Package.[27−30] A plane wave basis set[31] with an energy cut off of 400 eV was used in combination with the projector-augmented wave[32,33] method for calculating the interactions between the core and valence electrons. Exchange−correlation effects, including dispersion corrections, were treated with the vdw-DF2 functional.[34−38] All calculations were spin-polarized unless otherwise noted. Atomic forces were minimized to a tolerance of 0.04 eV/Å.

Calculations on bulk LCO were performed with a $6 \times 6 \times 6$ *k*-point mesh. It was verified that Co ions in the bulk adopt a

https://dx.doi.org/10.1021/acs.jpcc.0c07550
J. Phys. Chem. C 2020, 124, 24097−24104

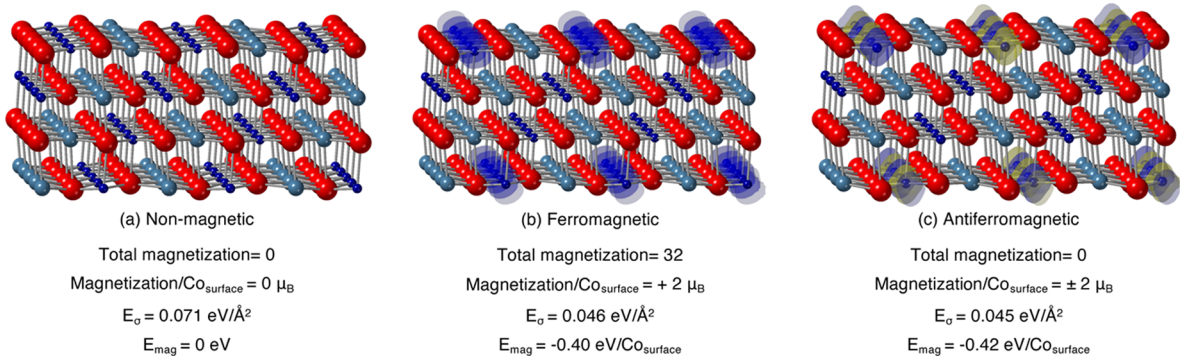

Figure 2. Energetic and magnetic properties of $(10\bar{1}4)$ LCO. Isosurfaces of magnetic spin density are shown for the (b) ferromagnetic and (c) antiferromagnetic orderings. E_σ represents the surface energy of the slab, while E_{mag} is the difference between the energies of the magnetic and nonmagnetic slabs, normalized by the number of surface Co contributing to magnetization. The blue (yellow) isosurfaces represent a positive (negative) magnetic moment at that location.

low spin state with no individual magnetic moments. Due to well documented self-interaction errors in the treatment of strongly correlated d shell electrons, a Coulombic correction, *U*, was applied to the Co ions' d-electrons following the approach of Dudarev.[39] A *U* value of 3.3 eV was used.[40]

The $(10\bar{1}4)$ surface of LCO has been reported in the literature as a low energy surface.[13−16] This surface also participates in lithium intercalation during battery charge/discharge.[13] While bulk LCO is nonmagnetic, it has been noted that the undercoordinated Co^{3+} ions on the $(10\bar{1}4)$ surface exhibit nonzero magnetic moments.[14−16,41,42] Our calculations suggest that these ions adopt an intermediate spin state with a magnetic moment of $\pm 2\ \mu_B$, consistent with earlier reports.[14,16] The presence of surface magnetism has the potential to both lower the surface energy and influence the nature of the interactions between the (magnetic) surface and adsorbed molecules. Consequently, a search over five different surface magnetic configurations was performed which include nonmagnetic, ferromagnetic, and three antiferromagnetic orderings. Three of these computational cells and their respective isosurfaces of the magnetic spin density are shown in Figure 2.

The computational cell used to model solvent decomposition reactions was constructed from a 4 × 4 expansion of the $(10\bar{1}4)$ surface unit cell. This cell has lateral dimensions of 11.40 Å × 11.27 Å and a vacuum region of 16.8 Å. These dimensions are sufficient to minimize spurious interactions between the periodic surfaces and images of the adsorbed solvent molecules. A four-layer slab was used, with the bottom two layers fixed at their bulk-like spacing. In total, each computational cell contained 128 LCO atoms; adsorption and decomposition calculations included an additional 10 atoms from EC. All calculations involving the 4 × 4 slab (with or without adsorbed molecules) were performed using a single *k*-point (1 × 1 × 1 mesh).

Adsorption energies were determined by $E_{ads} = E_{slab+EC} - E_{slab} - E_{EC}$, where E_{ads} is the adsorption energy, $E_{slab+EC}$ is the energy of the cell containing the adsorbed solvent molecule on the slab, E_{slab} is the energy of the pristine slab, and E_{EC} is the energy of the isolated solvent molecule. The energy of the isolated solvent molecule was calculated in an empty box; this energy was then augmented with the experimental vaporization enthalpy of EC,[43] 0.585 eV, to approximate the energy of EC in the liquid phase.

A subset of initial candidate adsorption configurations was generated using classical MC simulations, carried out in the adsorption module in Materials Studio. These calculations used a fixed surface slab geometry (generated from a prior DFT geometry optimization), the universal force field,[44] and partial charges determined by a Bader charge[45−48] analysis. As a relatively small molecule, EC has no distinguishing conformations; nevertheless, in the course of the MC calculations, the EC molecule was treated either as having a fixed geometry or one that could bend and distort based on energy minimization. The ten lowest energy configurations from both simulation types (fixed or flexible EC) were used as starting structures for subsequent DFT calculations. In addition to the MC-generated geometries, 18 configurations were created by hand and subsequently relaxed *via* DFT. In total, 38 candidate adsorption configurations for EC on LCO were explored. DFT calculations were performed on these geometries with and without spin polarization. Spin-polarized configurations initially assumed ferromagnetic ordering on the surface Co^{3+} ions. The 13 lowest energy and geometrically distinct configurations were further analyzed assuming an antiferromagnetic ordering.

Once the most likely intact adsorption configurations for EC were determined, possible decomposition pathways were examined by manually breaking one or two bonds in the EC; every bond in EC was explored in this manner except the double bond between O_C and C_C (see Figure 1). Several structures were created for each bond break by either positioning the fragmented ends near oppositely charged atoms on the LCO surface or extending them toward the vacuum region. These initial structures were then relaxed with DFT to determine more realistic configurations and assess their energy with respect to that of the intact structure. In cases where the resulting decomposition products yielded lower energy than the intact configuration, NEB[49,50] calculations were used to determine the reaction barrier. Linear interpolation was used to generate five images between the fully intact and fully decomposed state of EC on $(10\bar{1}4)$ LCO. Converging the NEB calculations was challenging due to spurious spin flips in the surface Co; spin flips result in sudden increases to the forces and energy of the impacted images.

RESULTS

Surface Magnetism. To determine the lowest-energy magnetic state of the $(10\bar{1}4)$ surface, surface energies were

https://dx.doi.org/10.1021/acs.jpcc.0c07550
J. Phys. Chem. C 2020, 124, 24097−24104

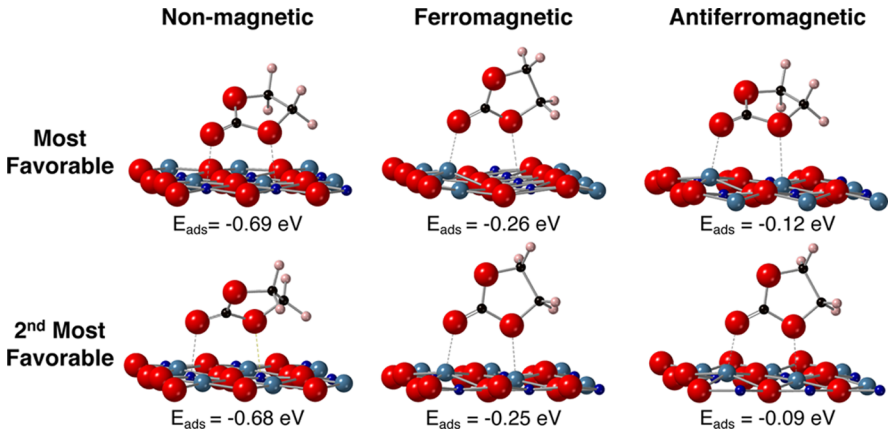

Figure 3. Most thermodynamically favorable adsorption geometries for nonmagnetic, ferromagnetic, and antiferromagnetic surfaces. E_{ads} is calculated by subtracting the energies of the clean slab and the isolated EC from that of the adsorption geometry. The vaporization enthalpy of EC is also accounted for; thus, E_{ads} represents the adsorption energy with respect to liquid EC.

evaluated for several magnetic orderings for the outermost Co^{3+}: a nonmagnetic state, a ferromagnetic intermediate spin state, and three antiferromagnetic intermediate spin states. Figure 2 compares the nonmagnetic, the ferromagnetic, and the lowest energy antiferromagnetic configurations on a 4 × 4 expansion of the surface. The magnetization density on each atom is displayed using isosurfaces. The magnetization is centered on the surface Co ions in both intermediate spin configurations. The antiferromagnetic and ferromagnetic configurations exhibit surface energies that are 37% and 35% lower, respectively, than that of the nonmagnetic surface. These results support the hypothesis that the formation of a distinct surface spin state stabilizes $(10\bar{1}4)$ LCO. As the antiferromagnetic configuration exhibited the lowest energy overall, this magnetic configuration is proposed as the most realistic surface model.

Nondissociative Adsorption of EC. To understand how the surface magnetic state impacts the adsorption of EC, adsorption geometries and energies were calculated on each of the nonmagnetic, ferromagnetic, and antiferromagnetic surfaces shown in Figure 2. The most energetically favorable adsorption geometries for each surface magnetic state are shown in Figure 3. In all cases, the most exothermic adsorption sites were found by situating the EC molecule so that the carbonyl and a ring O were positioned over cations on the LCO surface. Altering the magnetic state of the surface impacted both the adsorption energetics and the orientation of the adsorbed molecule. The nonmagnetic surface resulted in the most exothermic adsorption energies, −0.69 *versus* −0.26 and −0.12 eV for the most favorable ferromagnetic and antiferromagnetic cases, respectively. The nonmagnetic surface favors EC adsorption at surface Co sites, whereas the magnetic surface configurations favor adsorption at surface Li. This difference in site preference can be explained by differences in the electronic structure of the Co ions between the nonmagnetic and magnetic configurations. In the spin polarized, magnetic calculations, Co electrons occupy lower energy states than in the spin-averaged, nonmagnetic calculations. The higher energy of the nonmagnetic configuration implies that these electrons will be more reactive, resulting in stronger adsorption energies relative to the magnetic configurations. Since the Li ions are oxidized, regardless of the magnetic state, their electronic structure is largely unchanged by the presence/absence of magnetism. The changing site preference for adsorption as a function of spin polarization primarily reflects changes to the electronic structure of Co ions alone. Hence, the magnetic state of the slab quantitatively and qualitatively impacts how the EC molecule interacts with the surface.

Two previous studies of EC adsorption on LCO $(10\bar{1}4)$ employed different assumptions about surface magnetism and reported that the carbonyl and/or ring oxygen of EC preferred to adsorb adjacent to surface Co. Tebbe *et al.* reported an adsorption energy of −1.07 eV/molecule on a nonmagnetic surface, which is more exothermic than the −0.69 eV/molecule found here. The discrepancy in these energetics is at least partially due to the use of a different reference energy for EC: here, the adsorption energy is evaluated with respect to liquid-phase EC by accounting for the experimental vaporization energy; in contrast, Tebbe *et al.* used implicit and explicit solvation effects.[19] EC adsorption on the FM surface was also studied by Giordano *et al.*, who reported an adsorption energy of approximately −0.3 eV/molecule. This value is in good agreement with the −0.26 eV/molecule found here.[20] However, that study reported that EC preferred the surface Co site and referenced their adsorption energy with respect to gas-phase EC rather than to the liquid. In the present study, adsorption is observed to be more likely to occur on Li sites when surface magnetism is accounted for. The preference for Li sites may be significant because electrolyte reactions involving surface Li may inhibit Li intercalation or facilitate the formation of Li carbonate (or other reactions that consume Li).

Additional calculations were conducted to explore whether EC adsorption on an intermediate spin surface Co ion would reinstate the octahedral coordination found for bulk Co and thereby impose a low spin state. The adsorption energy increased (became more endothermic) when Co was constrained to a low spin configuration (see Table S1) when coordinated by EC. Hence, Co ions on both the ferromagnetic and antiferromagnetic surfaces prefer the intermediate spin configuration even when coordinated by EC. This suggests that adsorbed O does not interact strongly enough with surface Co to mimic the bulk octahedral coordination; the adsorption is more likely due to van der Waals and electrostatic interactions. Charge transfer, as analyzed with Bader charge calculations, confirmed this hypothesis, as only 0.03 electrons are transferred between the surface and the EC during adsorption.

https://dx.doi.org/10.1021/acs.jpcc.0c07550
J. Phys. Chem. C 2020, 124, 24097−24104

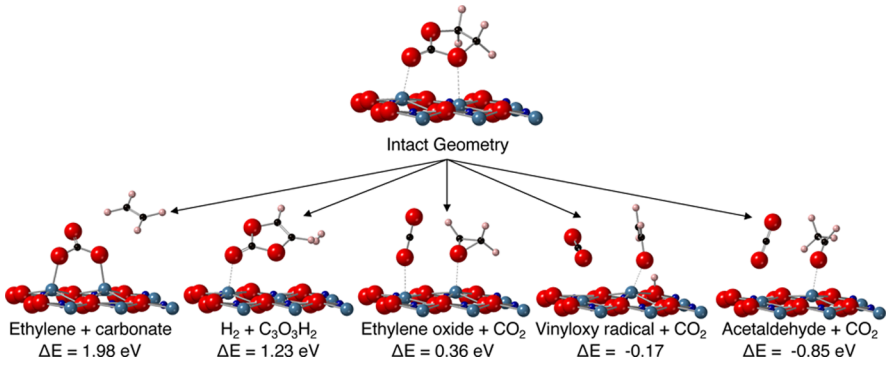

Figure 4. Selection of possible decomposed states of EC near $(10\bar{1}4)$ LCO. Five potential decomposition states and the energy difference from the intact state are shown. Two of the five are exothermic, suggesting that the decomposition may occur spontaneously.

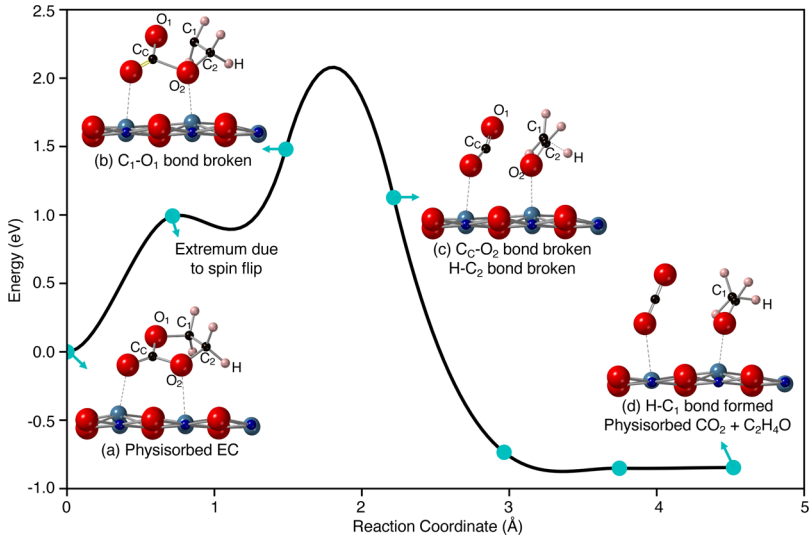

Figure 5. Energy profile for the decomposition of physisorbed EC (inset a) into CO_2 and C_2H_4O (acetaldehyde), computed at $T = 0$ K using the NEB method. The blue circles show the energy of the images used in the NEB calculation. The first maximum (at reaction coordinate ~0.8 Å) is due to spin fluctuations on Co on the inactive (opposite) surface of the slab and is not related to EC decomposition. Decomposition begins with the breaking of the C_1-O_1 bond (inset b), followed by both the C_C-O_2 and H_1-C_2 bonds, resulting in a physisorbed CO_2 molecule, fragmented C_2H_3O, and abstracted H (inset c). The abstracted H subsequently bonds with C_1, forming an acetaldehyde molecule that is physisorbed on the surface (inset d).

Decomposition Reactions. As the antiferromagnetic surface ordering is the most favorable energetically, the two lowest-energy antiferromagnetic intermediate spin geometries identified for intact adsorbed EC were adopted. These geometries are shown in Figure 3. Starting from these geometries, EC was subsequently decomposed into several potential reaction products, as described above. The relaxed geometries of these products are illustrated in Figure 4 for the lowest energy intact geometry (decomposition results for the second most favorable geometry follow the same trend). Upon relaxation, the structures of the candidate products either reverted to an intact EC or multiple (additional) bonds broke spontaneously, resulting in the products shown in Figure 4. For both initial intact adsorption geometries, two bond breaking events resulted in negative reaction enthalpies: moving a hydrogen to a surface oxygen (*i.e.*, proton abstraction) resulted in the formation of a vinyloxy radical (C_2H_3O) and CO_2, while breaking the C_1-O_1 bond produced acetaldehyde and CO_2. For both intact adsorption geometries, the formation of acetaldehyde and CO_2 was the most exothermic decomposition reaction, with reaction energies of −0.85 and −0.83 eV/molecule, respectively. In contrast, the reaction energies for proton abstraction and formation of the CO_2 + vinyloxy radical are much less exothermic, −0.17 and −0.13 eV/molecule.

Acetaldehyde and CO_2 are closed shell species that interact weakly with the surface. Importantly, both species are gaseous at or near room temperature and therefore may contribute to the accumulation of gas in the battery cell. The present findings are in good agreement with the experimental data, which report that the main gases produced by electrolyte decomposition in Li-ion batteries are CO_2, CO, and H_2[5,10,25] and that acetals are commonly identified at the cathode surface.[18]

To determine the impact of the $(10\bar{1}4)$ LCO surface upon EC decomposition, the reaction energy associated with gas-phase decomposition of isolated EC into (isolated) CO_2 and C_2H_4O was evaluated. This reaction was found to be endothermic, +0.89 eV/molecule, indicating that the LCO surface does play a role in the decomposition reaction.

Prior DFT studies have explored EC decomposition *via* deprotonation and ring opening pathways.[18−22,26] Tebbe *et al.* predicted that an EC molecule adsorbed on nonmagnetic surface Co decomposed to CO_2 and acetaldehyde with a reaction enthalpy of −0.5 eV.[19] Accounting for surface

https://dx.doi.org/10.1021/acs.jpcc.0c07550
J. Phys. Chem. C 2020, 124, 24097−24104

magnetism, the reaction enthalpy obtained here for the same products, −0.83 to −0.85 eV, is more exothermic. Giordano *et al.* found that deprotonation occurred with a reaction enthalpy of about −0.3 eV on a ferromagnetic $(10\bar{1}4)$ LCO surface.[20] Conversely, no exothermic deprotonation events were observed in the present study, unless accompanied by additional bond breaking and the formation of CO_2 and a vinyloxy radical. Additional EC ring opening events were observed with *ab initio* molecular dynamics on the $(11\bar{2}0)$ surface by Tamura *et al.*, suggesting that other surfaces and ring-opening mechanisms may play a role in EC decomposition.[21]

Reaction Barrier. NEB calculations were used to estimate the reaction barrier for the surface-mediated decomposition of EC into CO_2 and C_2H_4O. Figure 5 shows the energy profile of this reaction, starting from the intact adsorbed molecule (Figure 5a) and completing with the formation of CO_2 and acetaldehyde at the surface (Figure 5d) (it should be noted that the first local maximum in the energy profile does not necessarily reflect the energetics of this bond breaking event; this maximum primarily results from a simultaneous, unrelated spin flip on two Co ions located in the inactive lower surface of the slab. As previously mentioned, these magnetic instabilities were not uncommon and required careful convergence of the calculations). The first step in the decomposition pathway is the breaking of the C_1-O_1 bond (Figure 5b), which occurs with a barrier <1.5 eV. The next events in the decomposition reaction involve the breaking of the C_C-O_2 bond and the migration of a H from C_2 to C_1 (Figure 5c). The bond breaking portion of this event appears to be the rate-limiting step, with a barrier of 2.1 eV. Subsequent bond breaking and formation lower the energy of the system until a reaction enthalpy of −0.85 eV is reached. The relatively large size of the energy barrier observed here for EC decomposition agrees with previous DFT studies on the nonmagnetic surface of LCO, where a similar decomposition pathway with a reaction enthalpy of −0.5 eV and a barrier of 1.81 eV was found.[19] Prior studies report that the barriers for EC decomposition decrease as Li is removed from Li-ion cathodes.[22,26] Taking the trend reported in ref 22 as an example, one may speculate that the present barrier would decrease by 0.5 eV upon delithiation of 1/3 of the Li in LCO.

CONCLUSIONS

Electrolyte gassing remains an important degradation mechanism and safety concern in Li-ion batteries. The present study has used classical and first-principles calculations to characterize the thermodynamics and kinetics of electrolyte gassing reactions mediated by the $(10\bar{1}4)$ surface of a LCO cathode. Classical MC calculations were used to screen hundreds of potential geometries for EC adsorption on LCO. Additional geometries described in the literature or derived from chemical intuition were explored. Subsequently, the structure and energetics of more than 30 candidate geometries for EC adsorption were refined using DFT calculations.

Significant qualitative and quantitative differences in adsorption behavior were observed as a function of the magnetic state of the surface. The nonmagnetic surface exhibited the most exothermic reaction energetics and preferentially adsorbed EC on surface Co ions. Nevertheless, the high energy of the nonmagnetic surface suggests that it is the least likely magnetic configuration; rather, the antiferromagnetic surface was predicted to be the most energetically favorable. With this magnetic ordering, EC prefers to adsorb on surface Li sites. Adsorption on surface Co sites has been reported in several studies examining electrolyte decomposition on LCO; our results suggest that decomposition occurs at Li sites when surface magnetism is taken into account. The preference for Li sites may be significant because electrolyte reactions involving surface Li may inhibit Li intercalation or facilitate reactions that consume Li.

The thermodynamic driving force for EC decomposition was explored for the most favorable adsorption geometries on the antiferromagnetic surface. Over 30 different bond breaking scenarios were investigated with eight potential reaction products, yielding two exothermic reaction pathways. The most exothermic pathway resulted in the formation of CO_2 and C_2H_4O, in agreement with previous experimental results. The driving force for this reaction, −0.85 eV/molecule, is 1.7 eV/molecule more exothermic than that for the same reaction in the gas phase, highlighting the role of the LCO surface in mediating decomposition. Negligible charge transfer between the molecule and the surface suggests that the surface catalyzes the decomposition without actively oxidizing the EC.

NEB calculations revealed a barrier of 2.1 eV for the decomposition process, implying that the reaction is kinetically limited. While this reaction pathway is unlikely to be a major contributor to electrolyte gassing in the fully discharged state (corresponding to full lithiation of LCO), it is hypothesized that the rate of decomposition reactions will accelerate as the cathode is (partially) delithiated, that is, in the charged state.

ASSOCIATED CONTENT

Supporting Information

The Supporting Information is available free of charge at https://pubs.acs.org/doi/10.1021/acs.jpcc.0c07550.

Adsorption energies as a function of surface magnetic state and geometries of adsorbed EC (PDF)

AUTHOR INFORMATION

Corresponding Author

Donald J. Siegel − *Applied Physics Program, Mechanical Engineering Department, Materials Science & Engineering, and University of Michigan Energy Institute, University of Michigan, Ann Arbor, Michigan 48109, United States;* orcid.org/0000-0001-7913-2513; Email: djsiege@umich.edu

Author

Mallory R. Fuhst − *Applied Physics Program, University of Michigan, Ann Arbor, Michigan 48109, United States*

Complete contact information is available at: https://pubs.acs.org/10.1021/acs.jpcc.0c07550

Notes

The authors declare no competing financial interest.

ACKNOWLEDGMENTS

The authors acknowledge financial support from the U.S. National Science Foundation, grant CBET-1351482, and from Ford Motor Company. M.R.F. acknowledges support from the NSF Graduate Research Fellowship Program, grant DGE 1256260. Both authors acknowledge helpful discussions with Dr. Andy Drews from Ford Motor Company.

https://dx.doi.org/10.1021/acs.jpcc.0c07550
J. Phys. Chem. C 2020, 124, 24097−24104

REFERENCES

(1) Goodenough, J. B.; Kim, Y. Challenges for Rechargeable Li Batteries†. *Chem. Mater.* **2010**, *22*, 587−603.
(2) Aurbach, D.; Markovsky, B.; Salitra, G.; Markevich, E.; Talyossef, Y.; Koltypin, M.; Nazar, L.; Ellis, B.; Kovacheva, D. Review on Electrode-Electrolyte Solution Interactions, Related to Cathode Materials for Li-Ion Batteries. *J. Power Sources* **2007**, *165*, 491−499.
(3) Ceder, G.; Hautier, G.; Jain, A.; Ong, S. P. Recharging Lithium Battery Research with First-Principles Methods. *MRS Bull.* **2011**, *36*, 185−191.
(4) Roth, E. P. Abuse Response of 18650 Li-Ion Cells with Different Cathodes Using EC:EMC/LiPF6 and EC:PC:DMC/LiPF6 Electrolytes. *ECS Trans.* **2008**, *11*, 19−41.
(5) Roth, E. P.; Orendorff, C. J. How Electrolytes Influence Battery Safety. *Electrochem. Soc. Interface* **2012**, *21*, 45−49.
(6) Onuki, M.; Kinoshita, S.; Sakata, Y.; Yanagidate, M.; Otake, Y.; Ue, M.; Deguchi, M. Identification of the Source of Evolved Gas in Li-Ion Batteries Using 13C-Labeled Solvents. *J. Electrochem. Soc.* **2008**, *155*, A794.
(7) Berkes, B. B.; Schiele, A.; Sommer, H.; Brezesinski, T.; Janek, J. On the Gassing Behavior of Lithium-Ion Batteries with NCM523 Cathodes. *J. Solid State Electrochem.* **2016**, *20*, 2961−2967.
(8) Browning, K. L.; Baggetto, L.; Unocic, R. R.; Dudney, N. J.; Veith, G. M. Gas Evolution from Cathode Materials: A Pathway to Solvent Decomposition Concomitant to SEI Formation. *J. Power Sources* **2013**, *239*, 341−346.
(9) Wuersig, A.; Scheifele, W.; Novák, P. CO2 Gas Evolution on Cathode Materials for Lithium-Ion Batteries. *J. Electrochem. Soc.* **2007**, *154*, A449.
(10) Mendoza-Hernandez, O. S.; Ishikawa, H.; Nishikawa, Y.; Maruyama, Y.; Umeda, M. Cathode Material Comparison of Thermal Runaway Behavior of Li-Ion Cells at Different State of Charges Including over Charge. *J. Power Sources* **2015**, *280*, 499−504.
(11) Xu, K. Electrolytes and Interphases in Li-Ion Batteries and Beyond. *Chem. Rev.* **2014**, *114*, 11503−11618.
(12) Kumar, N.; Siegel, D. J. Interface-Induced Renormalization of Electrolyte Energy Levels in Magnesium Batteries. *J. Phys. Chem. Lett.* **2016**, *7*, 874−881.
(13) Kramer, D.; Ceder, G. Tailoring the Morphology of LiCoO2: A First Principles Study. *Chem. Mater.* **2009**, *21*, 3799−3809.
(14) Qian, D.; Hinuma, Y.; Chen, H.; Du, L.-S.; Carroll, K. J.; Ceder, G.; Grey, C. P.; Meng, Y. S. Electronic Spin Transition in Nanosize Stoichiometric Lithium Cobalt Oxide. *J. Am. Chem. Soc.* **2012**, *134*, 6096−6099.
(15) Hong, L.; Hu, L.; Freeland, J. W.; Cabana, J.; Öğüt, S.; Klie, R. F. Electronic Structure of LiCoO2 Surfaces and Effect of Al Substitution. *J. Phys. Chem. C* **2019**, *123*, 8851−8858.
(16) Han, B.; Qian, D.; Risch, M.; Chen, H.; Chi, M.; Meng, Y. S.; Shao-Horn, Y. Role of LiCoO2 Surface Terminations in Oxygen Reduction and Evolution Kinetics. *J. Phys. Chem. Lett.* **2015**, *6*, 1357−1362.
(17) Xu, K. Nonaqueous Liquid Electrolytes for Lithium-Based Rechargeable Batteries. *Chem. Rev.* **2004**, *104*, 4303−4418.
(18) Gauthier, M.; Karayaylali, P.; Giordano, L.; Feng, S.; Lux, S. F.; Maglia, F.; Lamp, P.; Shao-Horn, Y. Probing Surface Chemistry Changes Using LiCoO2-Only Electrodes in Li-Ion Batteries. *J. Electrochem. Soc.* **2018**, *165*, A1377.
(19) Tebbe, J. L.; Fuerst, T. F.; Musgrave, C. B. Degradation of Ethylene Carbonate Electrolytes of Lithium Ion Batteries via Ring Opening Activated by LiCoO2 Cathode Surfaces and Electrolyte Species. *ACS Appl. Mater. Interfaces* **2016**, *8*, 26664−26674.
(20) Giordano, L.; Karayaylali, P.; Yu, Y.; Katayama, Y.; Maglia, F.; Lux, S.; Shao-Horn, Y. Chemical Reactivity Descriptor for the Oxide-Electrolyte Interface in Li-Ion Batteries. *J. Phys. Chem. Lett.* **2017**, *8*, 3881−3887.
(21) Tamura, T.; Kohyama, M.; Ogata, S. Combination of first-principles molecular dynamics and XANES simulations for LiCoO2 -electrolyte interfacial reactions in a lithium-ion battery. *Phys. Rev. B* **2017**, *96*, 035107.
(22) Kumar, N.; Leung, K.; Siegel, D. J. Crystal Surface and State of Charge Dependencies of Electrolyte Decomposition on LiMn2O4-Cathode. *J. Electrochem. Soc.* **2014**, *161*, E3059−E3065.
(23) Kumar, N.; Radin, M. D.; Wood, B. C.; Ogitsu, T.; Siegel, D. J. Surface-Mediated Solvent Decomposition in Li-Air Batteries: Impact of Peroxide and Superoxide Surface Terminations. *J. Phys. Chem. C* **2015**, *119*, 9050−9060.
(24) Golubkov, A. W.; Fuchs, D.; Wagner, J.; Wiltsche, H.; Stangl, C.; Fauler, G.; Voitic, G.; Thaler, A.; Hacker, V. Thermal-Runaway Experiments on Consumer Li-Ion Batteries with Metal-Oxide and Olivin-Type Cathodes. *RSC Adv.* **2014**, *4*, 3633−3642.
(25) Jusys, Z.; Binder, M.; Schnaidt, J.; Behm, R. J. A Novel DEMS Approach for Studying Gas Evolution at Battery-Type Electrodel electrolyte Interfaces: High-Voltage LiNi0.5Mn1.5O4 Cathode in Ethylene and Dimethyl Carbonate Electrolytes. *Electrochim. Acta* **2019**, *314*, 188−201.
(26) Okuno, Y.; Ushirogata, K.; Sodeyama, K.; Shukri, G.; Tateyama, Y. Structures, Electronic States, and Reactions at Interfaces between LiNi0.5Mn1.5O4 Cathode and Ethylene Carbonate Electrolyte: A First-Principles Study. *J. Phys. Chem. C* **2019**, *123*, 2267−2277.
(27) Kresse, G.; Hafner, J. Ab initio molecular-dynamics simulation of the liquid-metal-amorphous-semiconductor transition in germanium. *Phys. Rev. B* **1994**, *49*, 14251−14269.
(28) Kresse, G.; Hafner, J. Ab initio molecular dynamics for liquid metals. *Phys. Rev. B: Condens. Matter Mater. Phys.* **1993**, *47*, 558−561.
(29) Kresse, G.; Furthmüller, J. Efficient iterative schemes for ab initio total-energy calculations using a plane-wave basis set. *Phys. Rev. B: Condens. Matter Mater. Phys.* **1996**, *54*, 11169−11186.
(30) Kresse, G.; Furthmüller, J. Efficiency of Ab-Initio Total Energy Calculations for Metals and Semiconductors Using a Plane-Wave Basis Set. *Comput. Mater. Sci.* **1996**, *6*, 15−50.
(31) Perdew, J. P.; Burke, K.; Ernzerhof, M. Generalized Gradient Approximation Made Simple. *Phys. Rev. Lett.* **1996**, *77*, 3865−3868.
(32) Kresse, G.; Joubert, D. From Ultrasoft Pseudopotentials to the Projector Augmented-Wave Method. *Phys. Rev. B: Condens. Matter Mater. Phys.* **1999**, *59*, 1758−1775.
(33) Blöchl, P. E. Projector Augmented-Wave Method. *Phys. Rev. B* **1994**, *50*, 17953−17979.
(34) Klimeš, J.; Bowler, D. R.; Michaelides, A. Chemical Accuracy for the van Der Waals Density Functional. *J. Phys.: Condens. Matter* **2009**, *22*, 022201.
(35) Lee, K.; Murray, É. D.; Kong, L.; Lundqvist, B. I.; Langreth, D. C. Higher-Accuracy van Der Waals Density Functional. *Phys. Rev. B: Condens. Matter Mater. Phys.* **2010**, *82*, 081101.
(36) Klimeš, J.; Bowler, D. R.; Michaelides, A. Van Der Waals Density Functionals Applied to Solids. *Phys. Rev. B: Condens. Matter Mater. Phys.* **2011**, *83*, 195131.
(37) Dion, M.; Rydberg, H.; Schröder, E.; Langreth, D. C.; Lundqvist, B. I. Van Der Waals Density Functional for General Geometries. *Phys. Rev. Lett.* **2004**, *92*, 246401.
(38) Román-Pérez, G.; Soler, J. M. Efficient Implementation of a van Der Waals Density Functional: Application to Double-Wall Carbon Nanotubes. *Phys. Rev. Lett.* **2009**, *103*, 096102.
(39) Dudarev, S. L.; Botton, G. A.; Savrasov, S. Y.; Humphreys, C. J.; Sutton, A. P. Electron-Energy-Loss Spectra and the Structural Stability of Nickel Oxide: An LSDA+U Study. *Phys. Rev. B: Condens. Matter Mater. Phys.* **1998**, *57*, 1505−1509.
(40) Wang, L.; Maxisch, T.; Ceder, G. Oxidation energies of transition metal oxides within theGGA+Uframework. *Phys. Rev. B: Condens. Matter Mater. Phys.* **2006**, *73*, 195107.
(41) Maram, P. S.; Costa, G. C. C.; Navrotsky, A. Experimental Confirmation of Low Surface Energy in $LiCoO_2$ and Implications for Lithium Battery Electrodes. *Angew. Chem., Int. Ed.* **2013**, *52*, 12139−12142.
(42) Sugiyama, J.; Nozaki, H.; Brewer, J. H.; Ansaldo, E. J.; Morris, G. D.; Delmas, C. Frustrated magnetism in the two-dimensional triangular lattice of Li_xCoO_2. *Phys. Rev. B* **2005**, *72*, 144424.
(43) Hong, C. S.; Wakslak, R.; Finston, H.; Fried, V. Some Thermodynamic Properties of Systems Containing Propylene

https://dx.doi.org/10.1021/acs.jpcc.0c07550
J. Phys. Chem. C 2020, 124, 24097−24104

Carbonate and Ethylene Carbonate. *J. Chem. Eng. Data* **1982**, *27*, 146−148.
(44) Rappé, A. K.; Casewit, C. J.; Colwell, K. S.; Goddard, W. A.; Skiff, W. M. UFF, a Full Periodic Table Force Field for Molecular Mechanics and Molecular Dynamics Simulations. *J. Am. Chem. Soc.* **1992**, *114*, 10024−10035.
(45) Sanville, E.; Kenny, S. D.; Smith, R.; Henkelman, G. Improved Grid-Based Algorithm for Bader Charge Allocation. *J. Comput. Chem.* **2007**, *28*, 899−908.
(46) Tang, W.; Sanville, E.; Henkelman, G. A Grid-Based Bader Analysis Algorithm without Lattice Bias. *J. Phys.: Condens. Matter* **2009**, *21*, 084204−84211.
(47) Henkelman, G.; Arnaldsson, A.; Jónsson, H. A Fast and Robust Algorithm for Bader Decomposition of Charge Density. *Comput. Mater. Sci.* **2006**, *36*, 354−360.
(48) Yu, M.; Trinkle, D. R. Accurate and Efficient Algorithm for Bader Charge Integration. *J. Chem. Phys.* **2011**, *134*, 064111.
(49) Henkelman, G.; Jónsson, H. Improved Tangent Estimate in the Nudged Elastic Band Method for Finding Minimum Energy Paths and Saddle Points. *J. Chem. Phys.* **2000**, *113*, 9978−9985.
(50) Henkelman, G.; Uberuaga, B. P.; Jónsson, H. A climbing image nudged elastic band method for finding saddle points and minimum energy paths. *J. Chem. Phys.* **2000**, *113*, 9901−9904.

https://dx.doi.org/10.1021/acs.jpcc.0c07550
J. Phys. Chem. C 2020, 124, 24097−24104